Stainless Steel with Tailored Porosity Using Canister-Free Hot Isostatic Pressing for Improved Osseointegration Implants

Hany Hassanin[1], Ali A. Al-Kinani[2], Amr ElShaer[2], Elena Polycarpou[2], Mahmoud Ahmed El-Sayed[3], Khamis Essa[4]*

[1] School of Mechanical and Automotive Engineering, Kingston University, UK, Email:h.hassanin@kingston.ac.uk
[2] School of Life Sciences, Pharmacy and Chemistry, Kingston University, UK
[3] Department of Industrial and Management Engineering, Arab Academy for Science and Technology and Maritime Transport, Abu Qir, Alexandria, Egypt.
[4] School of Engineering, University of Birmingham, UK,

Abstract

Porous biomedical implants hold great potentials in preventing stress shielding while improving bone osseointegration and regeneration. In this paper, a novel approach is introduced to control the porosity of 316L stainless steel implants by using canister-free hot isostatic pressing (CF-HIPing). The proposed approach uses cold isostatic pressing (CIPing) to generate powder compacts with various particle size, followed by CF-HIPing. 316L stainless steel samples with controlled porosity, mechanical and biological properties were successfully achieved. The results showed a significant increase in the samples porosity with increasing the powder size. Porous structures with strength of 108-360 MPa, Vickers hardness of 25-49 HV and elastic modulus between 17-50 GPa were produced using a particle size range of 5-50 µm. The effect of samples with various porosity on *in vitro* response of mouse pre-osteoblastic in terms of toxicity and proliferation was studied. All samples showed that they had a minimal toxic effect on the osteoblasts. Samples with low porosity, prepared using a particle size of 5 µm, is believed to hinder the transport of nutrients and oxygen to the cells hence had lower proliferation. In addition, samples prepared using a particle size range of 16-50 µm were associated with an increased proliferation and are therefore expected to improve the rate of bone osseointegration.

Keywords: Porous implants; Stainless Steels; Hot Isostatic Pressing; Cold Isostatic Pressing.

1. Introduction

The surge in demand for biomedical implants is fuelled by many factors such as the increase of the global population, implementation of better healthcare and ageing. With the rapid increase of the human population over the past decade, technologies to enhance healthcare quality have become abundant, particularly for individuals who suffer from chronic illness or traumatic injuries [1]. Osteoporosis is one of the most common diseases encountered in the elderly. It is a health condition associated with bone structural deterioration, and porous bone which increases the risk of fracture [2]. In the UK, around 3 million people suffer from osteoporosis. Despite the advancements in the screening tools and the early diagnosis of osteoporosis, bone fracture is common amongst geriatrics and affects 20% of males and 50% of females over the age of 50 [3]. Over the years, the demand for biomedical implants has increased, with global sales estimation of over $116 billion by 2022 with annual growth rate of 7.1% from 2016 to 2022. The orthopaedic implants sector is considered the highest revenue-generating segment in the biomedical implant market due to various reasons including aging, stressful lifestyle, unhealthy eating habits, and most importantly the development of advanced biomedical implants [4].

Surgeries involving orthopaedic implants have been well established for many years now. They are implemented to help people who suffer from joint and bone diseases. Nonetheless, around 10% of orthopaedic implant surgeries fail [5]; mainly because of fibrous encapsulation, infections and stress shielding caused by the elastic modulus mismatch between the bone and the implant [6]. In response to stress shielding, the osteoclast activity increases causing a reduction in the bone density and eventually is resorbed. Hence, metal materials with Young's modulus similar to that of the bone are preferred for manufacturing biomedical implants. Other properties such as corrosion, density, strength, radiolucency, thermal conductivity, melting point, and malleability are also important in selecting the implants' materials [7, 8].

Metals and alloys have superior structural and mechanical properties, nonetheless, the majority are susceptible to corrosion or biological reactions, leaving only a few suitable candidates for biomedical implants such as titanium and its alloys, cobalt-chromium alloys, ceramics, zirconium alloys and stainless steel [9-11]. Stainless steel 316L, also known as surgical stainless

steel is the recommended grade for surgical device manufacture [12]. It has excellent mechanical properties (strength and ductility), biocompatibility, pitting and crevice corrosion resistance due to the presence of chromium and molybdenum. Stainless steel 316L has an elastic modulus of 193 GPa, which is 6- 20 times greater than human bone elastic modulus, making stainless steel 316L implants susceptible to failure by stress shielding. Moreover, it decreases the interfacial bond between the solid implant and the surrounding tissues [13]. Introducing porosity into metals and alloys can be used as an effective strategy to reduce their elastic modulus. As such, the development of porous implants could be an effective technique to address these concerns, by controlling the porosity content and hence the stiffness of the implant to match the bone's stiffness [14-17]. In addition, a porous biomedical implant allows an excellent environment for body fluids and drugs to flow effectively through the porous network. This therefore offers better opportunities for the body tissue to grow and enhance osseointegration and bone regeneration by providing a good interfacial bonding between the implant and bone [18-20].

Recently, manufacturing processes of highly porous materials have gained much attention especially for biomedical applications. Powder metallurgy and sintering of compacted powders is one of the common approaches that have been used to fabricate porous parts [21, 22]. Space holders or foaming agents have also been investigated for their potential ability to create porous materials [23, 24]. Nonetheless, impurities and contaminations limit the use of this process for biomedical applications, where using materials with extra low interstitials is typically required. The most commonly used methods to produce highly porous biomaterials are gas foaming, salt leaching, freeze-drying, and phase separation depending on the material used to manufacture the scaffold structure [25-27]. Injection moulding combined with a space holder process was also investigated for the production of structures with highly porous parts. Injection moulding offers rapid and mass production with low labour cost and waste. However, the tooling cost and the design restrictions limit the use of this technique for biomedical applications. Another limitation is the high reactivity of metals during de-binding, resulting in production of parts with high interstitial content [28]. Recently, developments in additive manufacturing have offered unprecedented opportunities for manufacturing structures to meet the high demands for biomedical implants [29, 30]. However, limitations of AM processes, such as overhanging

structures, supporting structure removals, post processing techniques, materials sustainability, inspection, and quality control need to be addressed for future applications [31].

Hot Isostatic Pressing (HIPing) is a heat treatment process where high pressures and high temperatures act simultaneously on metal or ceramic parts to eliminate porosity and achieve full density and isotropic properties [32, 33]. HIP is considered as a high performance and viable option to conventional methods such as machining, casting and metal forming in different applications [34]. HIP is currently used as a post process to further densify porous components or as a net shape process to consolidate powder. It is also used as a diffusion bonding technique for joining parts. It can bind to similar or different materials using the simultaneous effect of the isostatic gas pressure and high temperature [35]. In a typical HIP process, a metal or a glass canister is being prepared with a cavity representing the design of the desired shape. The initial geometry of the canister has to be well designed to compensate the shrinkage during the process. The canister is subsequently filled with metal powder, packed using vibratory table to achieve powder with uniform density, outgassed for 24 hours, and sealed by hot crimping [36, 37]. After HIPing the canister, chemical leaching or machining is employed to remove and achieve the HIPed Part. Currently, a plethora of research has been reported on HIP for aerospace and automotive applications while only a few reports explored HIP in biomedical applications [35]. This could be attributed to the high cost associated with HIP compared to conventional techniques. Manufacturing and removal of the HIP sacrificial canisters are large contributors to the high cost of HIP parts and restricts their complexity. Haan et al. investigated the effect of HIP on the properties of additive manufacturing parts. It was reported that fatigue properties of selective laser melting cobalt-based implants were significantly enhanced by using HIP. Selective laser melting samples typically exhibit a significant amount of porosity and defects. Hence, applying HIP post process helps to eliminate porosity and improve the implant mechanical properties [38]. HIP was also used to promote hydroxyapatite (HA) coatings by creating a strong bond on a titanium implant [39, 40]. Furthermore, HIP was implemented for the densification of zirconia implants with improved fatigue properties [41].

In this paper, the typical HIP process was modified by not using a canister for powder

capsulation. Hence, porosity was promoted and could potentially be used in low-stiffness implants. In addition, HIPing without a canister, a canister free HIPing (CF-HIP), can significantly reduce the overall cost of the process. Wet bag cold Isostatic Pressing (CIP) was used to prepare the stainless steel green parts by applying isostatic pressure on soft moulds filled with stainless steel powder. Afterwards, the compacted parts were subjected to HIPing without using a canister. Different particle sizes were used in the experimental work and the influence of the mean particle size on the properties of the HIPed samples were investigated. Because implants are designed to be in intimate contact with living cells and tissues, implants should improve bone regeneration. Therefore, biocompatibility characterisation was used to evaluate the cytotoxicity and to investigate the influence of the process on the growth and proliferation of the bone cells.

2. Experimental

2.1. Powder, CIP and CF-HIP

Stainless steel 316L powder was supplied by Sandvik Osprey, UK. Four different particle sizes were investigated with mean particle sizes (D_{50}) of 5, 10, 16 and 50 µm. Table 1 shows the composition of the supplied powder. The received powders were examined using Scanning Electron Microscopy (SEM) to assess their morphology. SEM images of the powders are shown in Figure 1. The figure shows that the majority of the particles have a spherical morphology in the various sizes, which helps produce a high packing density due to the ease of the powder flow.

Table 1: Composition of the 316L powders

Element	Fe	Cr	Ni	Mo	Mn	Others
Percentage (%)	Balance	16.5	10.5	2.1	1.5	0.9

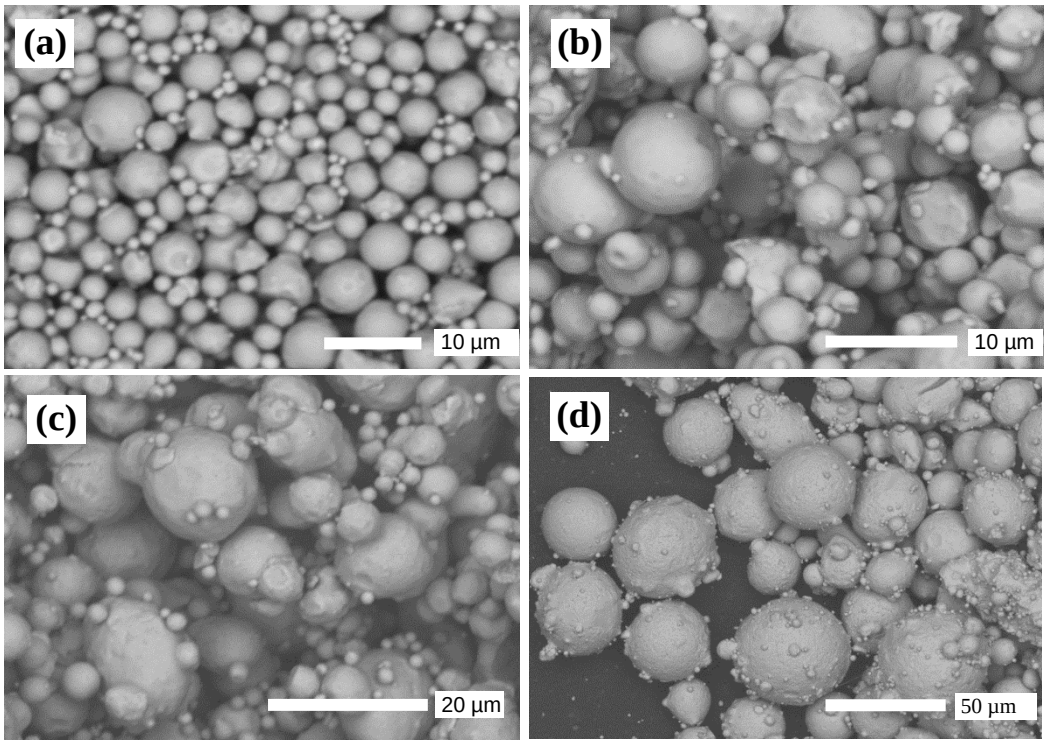

Figure 1: SEM images of the stainless steel 316L powder with mean particle sizes of (a) 5 µm, (b) 10 µm, (c) 16 µm, (d) 50 µm.

Wet bag CIPing was carried out to compact the four stainless steel powders. The reason for using CIP to compact the stainless steel 316L powder is that it does not need any additives to achieve uniform compacts. In order to prepare the samples, soft moulds made from Polydimethylsiloxane (PDMS) were first produced. Cylindrical-shaped cavities of different sizes were prepared to assess the mechanical and physical properties of the samples. PDMS prepolymer (Sylgard 184-Dow, Corning Corp.) consists of two parts (a base material and a curing agent). Glass or metal cylinders representing the samples dimensions were placed onto a plastic substrate. Next, the plastic substrate holding the cylinders was placed onto an aluminium container as shown in Figure 2a. The PDMS base material and the curing agent were mixed thoroughly using a mechanical stirrer with a weight ratio (base to curing agent) of 10:1. The mix was de-aired in a vacuum chamber to remove any trapped bubbles. After de-airing, the mixture was poured onto the mould and de-aired again. The mould was cured at 70 °C for 3 hours. After cooling, the cured soft mould was peeled off from the master mould as shown in Figure 2b. The prepared soft moulds shown in Figure 2c were filled with as-received powders using a vibratory table to achieve a uniform and good packing of the powder. Next, the soft moulds were sealed

using a PDMS lid and placed in a rubber bag. The rubber bag was then placed inside the CIP cylinder and filled with water, prior to pressurising the cylinder to 60 MPa. The pressure was left to stabilize over 5 minutes before gradually releasing the valve. The rubber bag was then removed to extract the green compacts, see Figure 2d. The green CIPed compacts were subsequently HIPed using a canister-free method (i.e. without canister). This means that the CIPed samples were placed in the HIP cylinder, followed by increasing the temperature and the pressure according to the HIP cycle. The cycle involved simultaneous application of temperature and pressure to 920˚C and 103 MPa, respectively, followed by an isothermal dwell at 920˚C of 2 hours, and finally furnace cooling to room temperature.

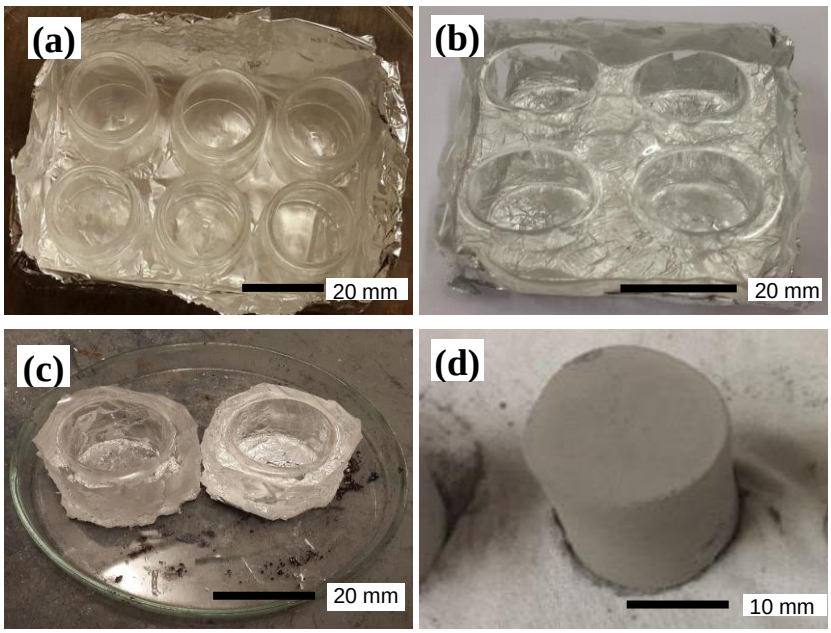

Figure 2: (a) master mould, (b) soft moulds, (c) soft mould ready for CIP, (d) CIPed sample.

2.2. Microstructural and Mechanical Characterisation

The aim to use four particle sizes in the preparation of the HIPed samples is to investigate the effect of the particle size, hence porosity, on the microstructural, mechanical, and biological properties of the samples. The powder apparent density was measured using the hall flowmeter funnel of free flowing powder following the guidelines of ASTM B212 [42]. On the other hand, density of the bulk CIPed compacts was measured using the mass to volume ratio. The mass was measured using an electronic balance supplied by Nimbus Precision while the volume of CIPed samples was calculated using $\pi/4\times D^2\times h$ where D and h are diameter and height, respectively.

The HIPed samples were ground, polished and cleaned using ultrasonic cleaning for microstructure characterization. A Hitachi TM3000 desktop Scanning Electron Microscope (SEM) and an optical microscope were used to characterize the porosity and the microstructure of the samples. Micrographs from the HIPed samples were taken at several locations across the polished sample surface. Porosity size and distribution were achieved by quantitative imaging analysis (using ImageJ®) of the polished samples. A JEOL7000 SEM was used to investigate the influence of the particle size on the microstructure of the samples. In addition, the samples were scanned by using a Bruker Skyscan1172 micro-computer tomography (micro-CT), with a maximum X-ray energy of 80 kV, 8 W beam power, 570 ms exposure per projection, aluminium and copper filter, and 3.4 μm pixel size to check the level of porosity within the HIPed samples. The scanned data were reconstructed into a 3-dimensional volume using NRecon Software (Bruker) [43], producing images with a spatial resolution of ~5 μm. Following reconstruction, the image analysis and thresholding were performed by CTan module (Bruker). 3D visualisation of surface connected and enclosed porosity was performed over selected volume of interest using CTVol module (Bruker). For all four samples, region of interest was selected across 1000 slices placed in the middle of the longitudinal axis (y-axis) of the samples to create volume of interest. Micro-hardness measurements were performed on polished surfaces of the samples using an INDENTEC hardness tester with a Vickers pyramid indenter and a load of 10 kg. In addition, compression test samples were machined out from the HIPed parts (5 samples per condition), with a square cross section of 5 mm × 5 mm and a length of 10 mm. The testing was conducted using ESH Servo Hydraulic Machine, with a strain rate of 1 mm/min^1.

2.3. *In vitro* Biocompatibility

2.3.1 Neutral Red Cytotoxicity Assay

The four HIPed samples were machined to a disk shape with diameter of 5 mm and thickness of 2 mm for the biocompatibility study. The Stainless steel 316L implants were cleaned using deionized water then soaked in absolute ethanol for 15 minutes. All implants were sterilized by exposing to ultraviolet light for 4 hours prior to the biological testing. The toxicity of the four implants was evaluated using mouse pre-osteoblastic cell line (MC3T3-E1; Preosteoblast; Mouse, ECACC). MC3T3 cells were cultured in Minimum Essential Medium α (Gibco™ MEM

α Nucleosides, No Ascorbic Acid Fisher Scientific) supplemented with 10% Fetal Bovine Serum (Fisher Scientific), and penicillin-streptomycin (Penicillin-Streptomycin with 10,000 units penicillin and 10 mg streptomycin per mL in 0.9% NaCl, (Sigma Aldrich UK). The cells were incubated at 37°C under 5% CO_2. After reaching 80% confluence, cells were detached using Trypsin-EDTA solution 0.25%, (Sigma Aldrich UK), centrifuged, and re-suspended.

For the neutral red assay, cells with passages between 6-10 were used. After sterilization, the samples were carefully transferred into a 24-well plate containing 50,000 cells per well at a final volume of 400µL. MC3T3 cells in the presence of the implants were incubated for 24 hrs at 37 °C with 5% CO_2. The growth media was then discarded carefully, to avoid disturbing or moving the insert, and the wells were washed twice with 300 µL of PBS followed by the addition of 200 µL of FBS free media containing neutral red (40 µg/mL). The plate was incubated at a temperature of 37 °C with 5% CO_2 for 2 hrs after which the neutral red solution was discarded and the plate was washed with 300µL PBS. The plate was de-stained using 200 µL of the de-stain solution made up of 50% ethanol and 1% acetic acid, and then was placed in a plate shaker for 3 minutes. Finally, the optical density of the extracted dye was measured at 540nm. The cell viability was calculated as mean OD value normalised to the negative control OD. Statistical significance was determined using one-way ANOVA of 3 independent experiments using GraphPad Prism (version 7.03).

2.3.2 Real-Time Imaging

The effect of the inserts on MC3T3 cells was observed in real time using an IncuCyte ZOOM® system. UV sterilised samples were carefully placed into a 24 well plate. Into each well, 400 µL of MC3T3 cell suspension were added (50,000 cells/well). Then, the plate was transferred into the IncuCyte ZOOM® (Essen Bioscience, UK) accommodated inside a conventional cell incubator set at 37 °C with 5% CO_2. Phase contrast images from each well were captured over 24 hours (at 2 hour intervals) using the 10x objective lens. The obtained images were analysed using IncyCyte Zoom 2015A GUI and the cell confluency vs time curve was constructed. Independent experiments were repeated 3 times.

3. Results and Discussions

Effect of the particle size on the apparent, CIPed, HIPed densities is shown in Figure 3. As shown in the figure, the apparent densities of the powder are 41.4%, 47.2%, 50.3% and 53.5% for particle size 5, 10, 16 and 50 µm, respectively. It can be noted that, the apparent density of the powder increases as particle size increases. When the particle size increases, the friction and adhesion forces between particles reduces which lead to a better powder flowability and thus higher powder packing. On the other hand, densities of the CIPed compacts were enhanced after conducting CIP. Similar to the apparent density, the CIPed density of the samples increases as particle size increases. In particular, the densities of the CIPed compacts were 54.1%, 58.0%, 60.2% and 63.1% for particle size 5, 10, 16 and 50 µm, respectively. Here, the CIPed density of the smallest particle size (5µm) increased by 12.7% while the CIPed density of the largest particle size (50µm) increased by 9.6%. In this case, when the particle size was decreased, the apparent density also decreased, and more space was available for particles rearrangement during CIPing. Hence, the applied pressure during CIP overcame the friction between particles and improved the density. In contrary to the apparent and CIPed densities, the density of the HIPed samples was decreased when the particle size increased. The density of the HIPed samples was 98.6%, 89%, 87.1% and 74.6% for particle size 5, 10, 16 and 50 µm, respectively. In order to understand the effect of the particle size on the densification of the samples, the microstructure of the CF-HIPed samples was characterised. Figure 4 shows the SEM micrographs of the microstructure of the CF-HIPed samples. The figure shows cross sections of the four developed 316L samples following CF-HIPing. As shown, different levels of densification are clearly visible which is believed to be caused by diffusion bonding of powder particles. When powder particle size decreases (Figure 4 a), a high bonding level between particles is achieved because of the short diffusion paths which leads to better densification. On the other hand, the presence of large open channels between coarse particles allows the gas pressure during CF-HIPing to penetrate and reduce diffusion bonding of powder particles, which leads to the presence of a large amount of porosity (Figure 4 d). The size of the channels between the particles generally increases with the increase in powder size.

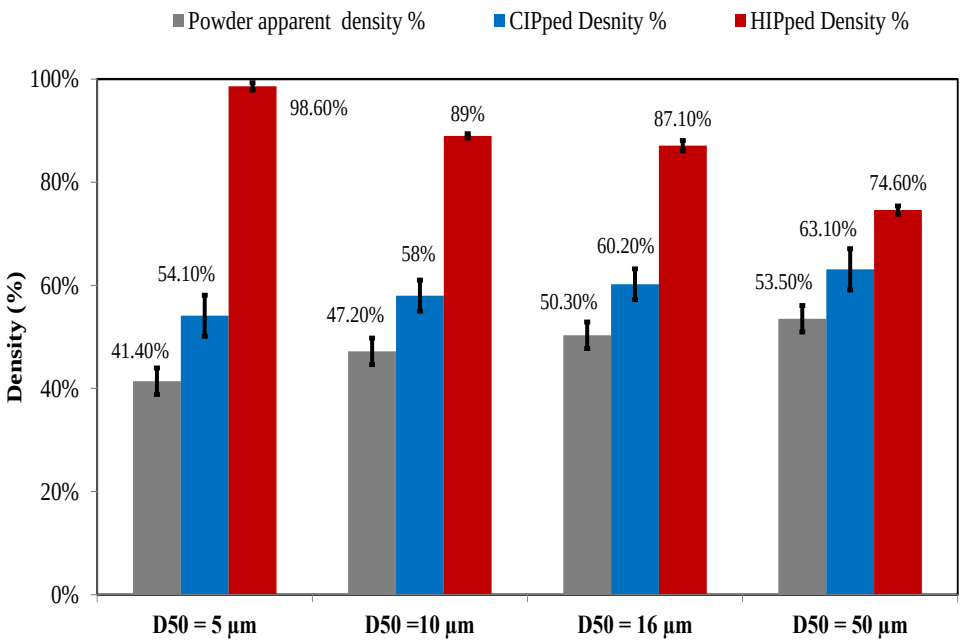

Figure 3: Apparent, CIPped, HIPed densities of samples prepared using powders with mean particle size diameter of 5 µm, 10 µm, 16 µm, and 50 µm.

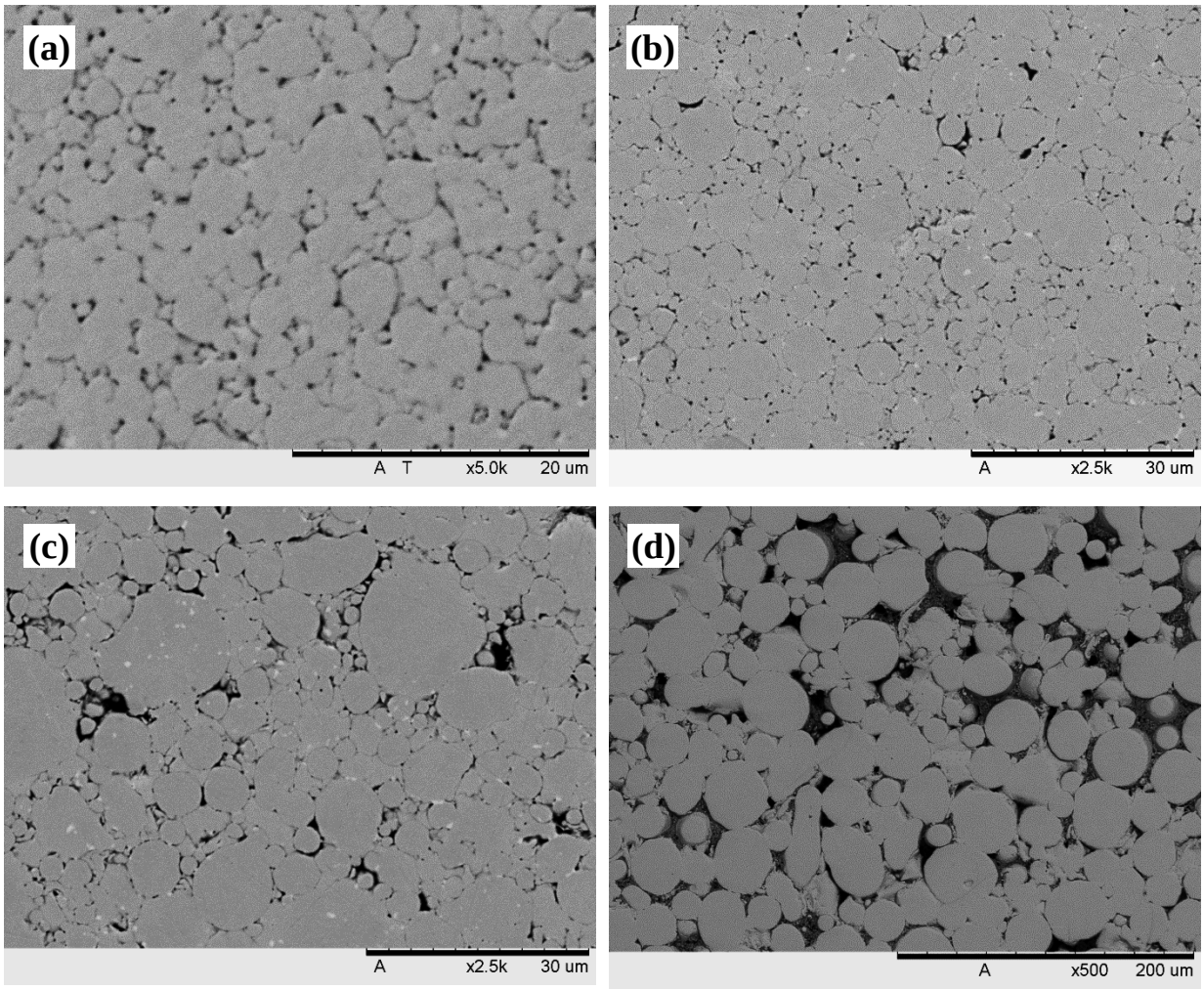

Figure 4: SEM micrographs of the cross sections of porous 316L CF-HIPed samples of different particle sizes: (a) 5 µm, (b) 10 µm, (c) 16 µm and (d) 50 µm.

To characterise the porosity of the CF-HIPed samples and the morphology of consolidation, micro-CT was performed to quantify the 3D variation in total porosity (surface connected and enclosed) using samples extracted from the core of the four particle size. In micro-CT, an open pore (surface connected) is defined as any pore found within a solid part or between solid objects, which has a connection in 3D to the pores outside the parts. Closed pore (enclosed) in 3D defined as a pore (black) voxels that is fully enclosed on all sides in 3D by solid (white) voxels. Total porosity and pore size range have been distinguished, visualised and quantified (Table 2 and Figure 5). It is evident that there is an increase in the level of open porosity when the particle size of the starting material increased. The results also show that highly porous structures can be achieved when a coarse powder is used while almost fully dense structures are obtained when powders of fine size are used in CF-HIP approach.

Table 2: Quantitative analysis of total, surface connected and enclosed porosity and pore size range within the samples prepared with different particle size.

Particle size (μm)	**5**	**10**	**16**	**50**
Total porosity (%)	1.4	11.0	12.9	25.4
Surface connected porosity (%)	0.1	8.5	11.2	24.97
Enclosed porosity (%)	1.3	2.7	1.9	0.40

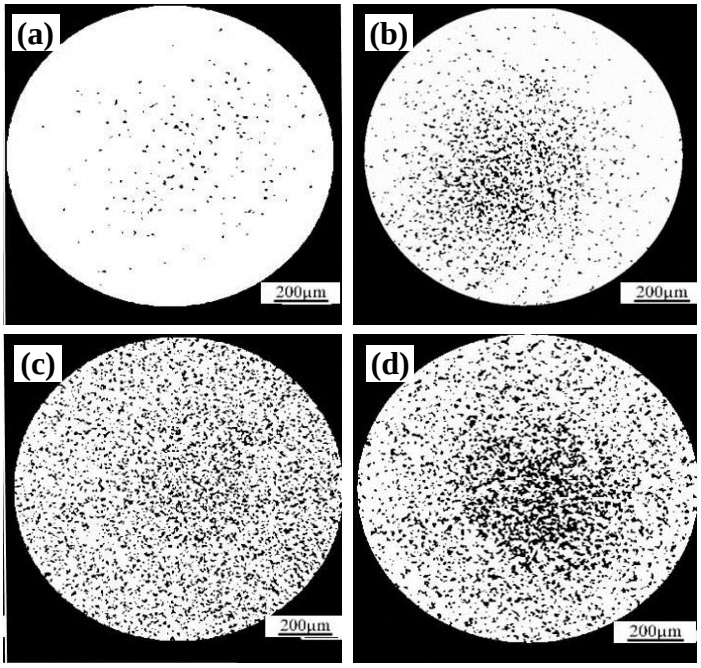

Figure 5: Binarised view of CF-HIPed porosity for samples prepared using particle size of (a) 5 μm, (b) 10 μm, (c) 16 μm, (d) 50 μm.

It is well established that HIPing cannot consolidate surface connected pores. Therefore, it is useful to understand the CIP efficiency in sealing internal porosity by characterising the surface of the CF-HIPing samples. Figure 6 shows SEM images of the CF-HIPed samples focusing on the surface layer of the samples. As shown in Figure 6, in all samples, the surface of the CF-HIPing samples shows a highly porous surface, with porosity approaching 30-50%. The thickness of the porous layer varied from ~80 μm, for samples prepared by 5 μm particle size, to ~ 350 μm for those using 50 μm powder size. However, within the compact itself, the pore fraction increased to the ranges shown in Table 2.

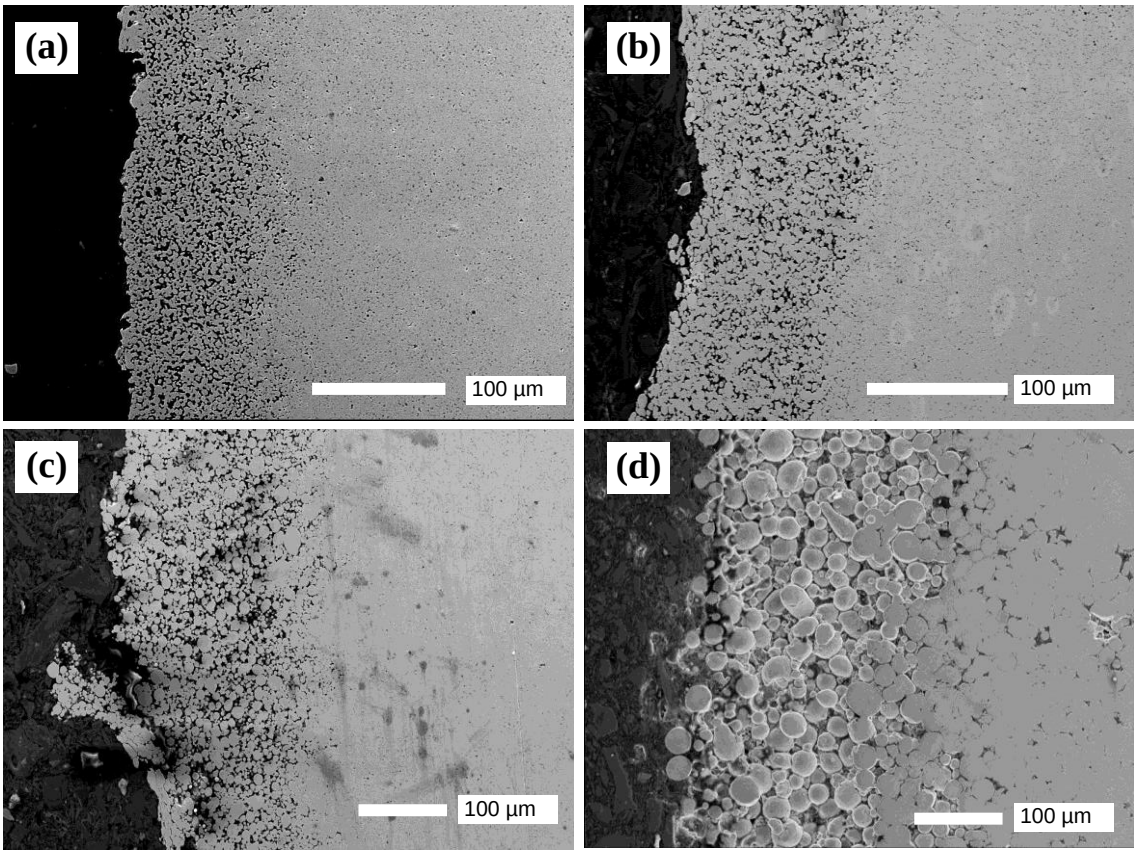

Figure 6: SEM images of the surface layer of the 316 L HIPed samples synthesised using a particle size of a) 5 µm, b) 10 µm, c) 16 µm and d) 50 µm

Figure 7, Figure 8 and Figure 9 show the effect of the porosity (in addition to the particle size) on compressive strength, Young's modulus, and micro-hardness of the CF-HIPed samples. It also compares the measured properties with the typical properties of 316L solid samples [44]. In general, all the aforementioned properties declined with the decrease of the porosity (increase in particle size). Samples with a particle size of 5 µm showed the lowest porosity of 1.4% and hence the highest combination of mechanical properties (360 MPa ultimate compressive strength, Young's modulus of 50 GPa, and hardness of 49 HV). On the other hand, increasing the porosity content to 25.4% for particle size of 50 µm was accompanied by an obvious decline in these properties to reach 108 MPa, 17 GPa, and 25 HV, respectively. Additionally, the compressive strength of samples prepares using particle size of 50 µm was similar to the typical compressive strength of 316L samples [44]. As described above the particle size of the powder has an impact on the morphology of the pores and the porosity fraction. In turn, these factors control the mechanical properties of the CF-HIPed materials. It could be clearly shown from Figure 3 that the percentage porosity increases as the particle size increases which has a detrimental

influence on the mechanical properties of the material. The best approach is to optimise Young's modulus-to-porosity % ratio is to match bone properties through using a particle size that could produce the desired values for the Young's modulus and porosity %, see Figure 7 .

Based upon the presented results, a particle size of 43 µm would be the optimum size for the desired application, as it would result in Young's modulus of 22 GPa, which is in the range of those of human bone's, and a porosity fraction of 22%. At these conditions, the compressive strength, ductility and hardness would be 147 MPa, 21.5% and 27 HV, respectively. As such, the mechanical properties of the CF-HIPed structures are likely to rely on the density of the consolidated component.

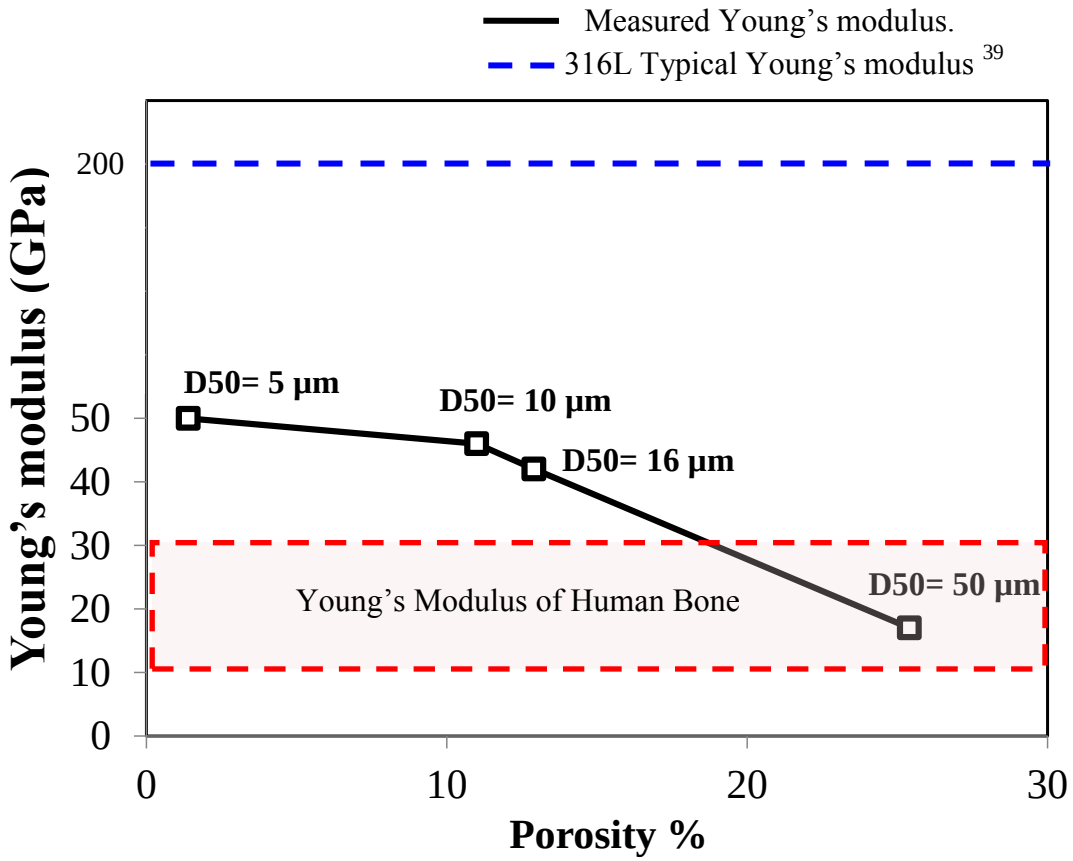

Figure 7: Effect of porosity on the Young's modulus of 316L CF-HIPed samples.

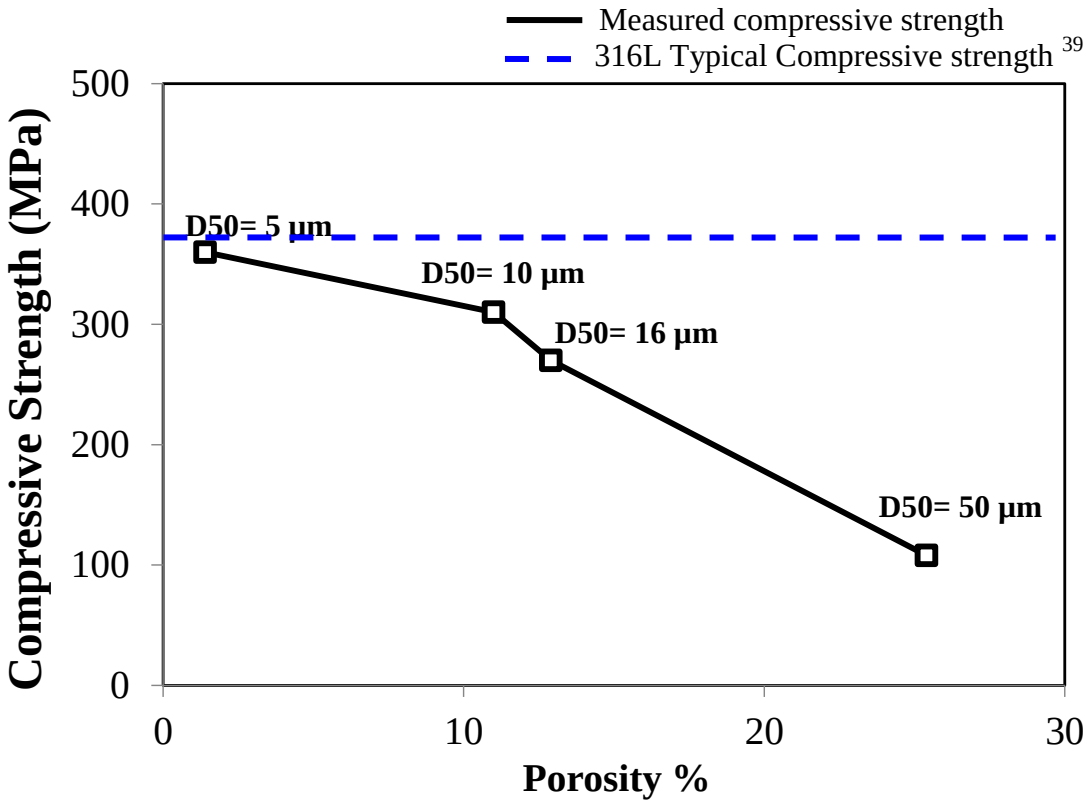

Figure 8: Effect of porosity on the compressive strength of 316L CF-HIPed samples.

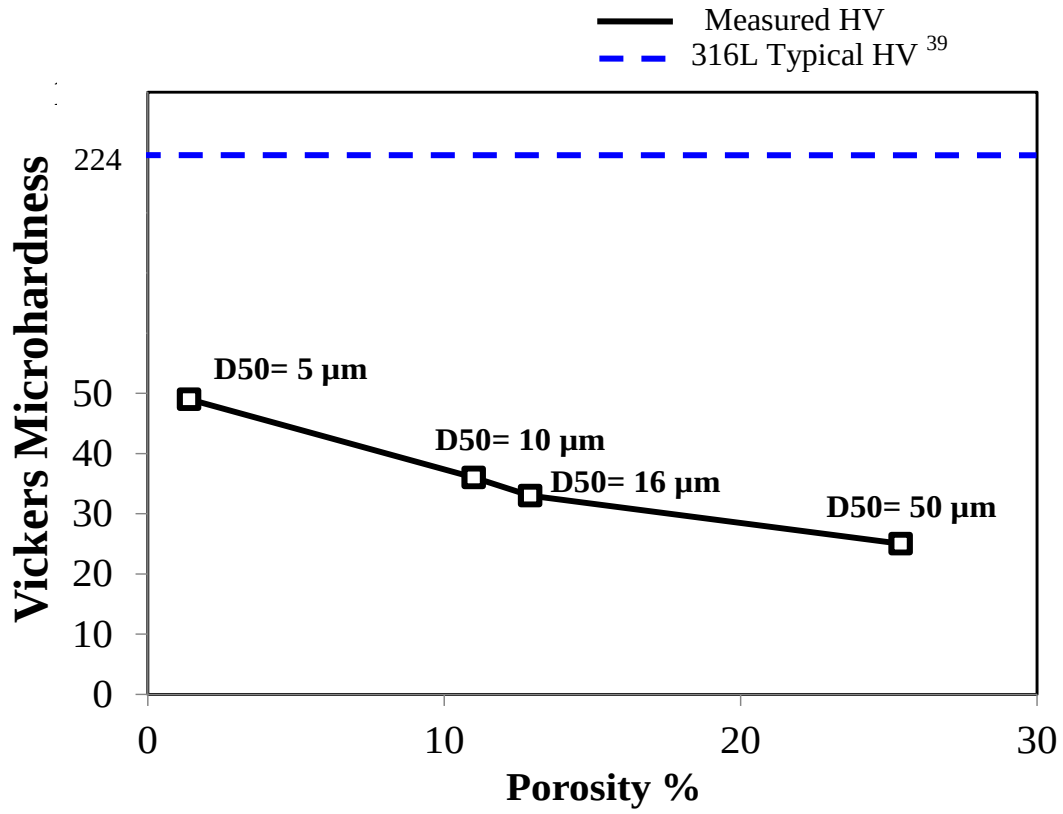

Figure 9: Effect of porosity on the Micro hardness of 316L HIPed samples.

3. Biocompatibility

To evaluate the toxicity of the four CF-HIPed samples, a neutral red uptake assay was used. The Neutral red cytotoxicity assay is widely used in biomedical applications to quantify the viable cells in the culture. Only viable cells will be able to uptake the neutral red dye in their lysosomes via active transport [45].

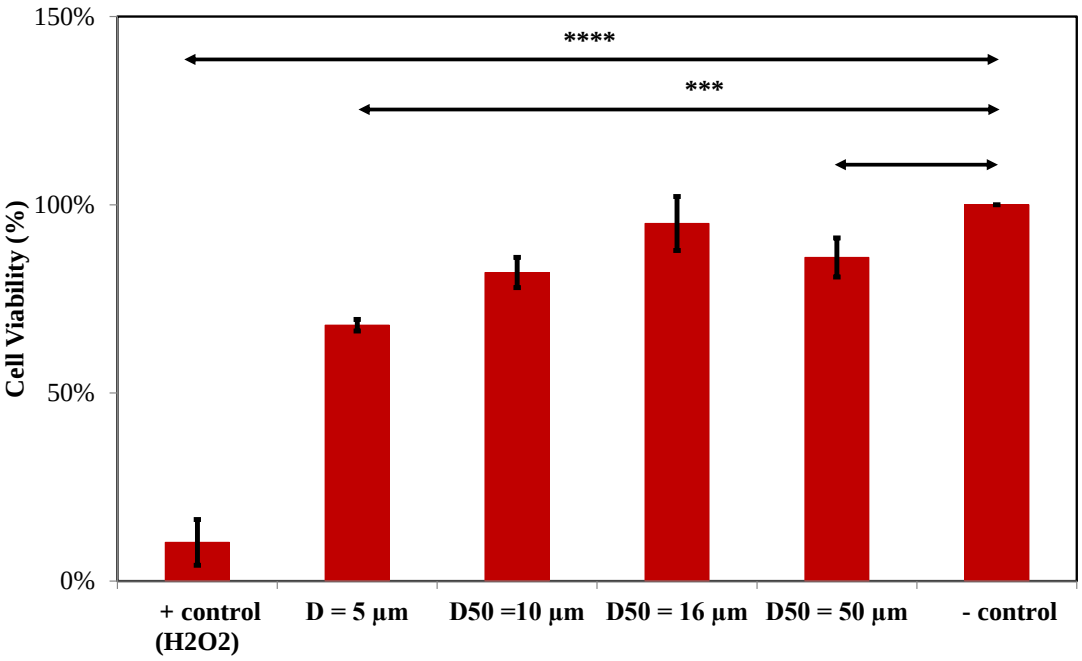

Figure 10: MC3T3 percent viability in the presence of CF-HIPed samples synthesised using a particle size of 5 µm, 10 µm, 16 µm , 50 µm , negative control (media only) and positive control (H2O2). Results are expressed as mean values of 3 independent experiments ±SD. ** $p<0.01$, *** $p<0.001$ and **** $p<0.0001$ as determined by one-way ANOVA and Tukey's multiple comparison test using GraphPad Prism 7.03

The cytotoxicity data is summarized in Figure 10. All the prepared CF-HIPed samples were found to have a minimal toxic effect on the MC3T3 cells. The neutral red cytotoxicity data showed that all CF-HIPed samples were biocompatible with significantly less toxic effect on the viability of the cells when compare to toxic agents such as hydrogen peroxide ($p<0.0001$). Nonetheless, one of the four formulations namely CF-HIPed samples of 5 µm had a significant effect on the viability of the cells compared to the negative control (Figure 12& Figure 12). Osteolysis or bone loss occurs when the balance between bone formation and bone resorption is affected. The decrease of peri-implant bone formation will be associated with osteolysis. In order to assess the peri-implant osteoblasts' growth, an incucyte ZOOM® was used to visualize

the proliferation patterns of MC3T3 cells in the presence of the CF-HIPed implants.

Both pore size and total porosity of bone implants are key factors in bone formation both *in vivo* and *in vitro*. It is believed that low porosity inhibits cell proliferation and forces cells to aggregate which stimulate osteogenesis. On the contrary, implants with large pores and high porosity content enhance bone ingrowth. The micro-CT data demonstrated that coarse particles formed highly porous structures with total porosity of 25.4% when particles of 50 µm were used. Seeding MC3T3 cells onto the stainless steel scaffolds showed a slow proliferation profile for CF-HIPed implants prepared with 5 µm particles. After 5 hours of seeding, less than 50% phase object confluence was achieved around the stainless steel implants. The confluence percentage increased to 57%, 67% and 56% for CF-HIPed implants made of 10, 16 and 50 µm respectively. The highest confluence percentage was observed in CF-HIPed implants made of particle size of 16 µm followed by implants made of particle size of 50 µm after 24 hours of seeding.

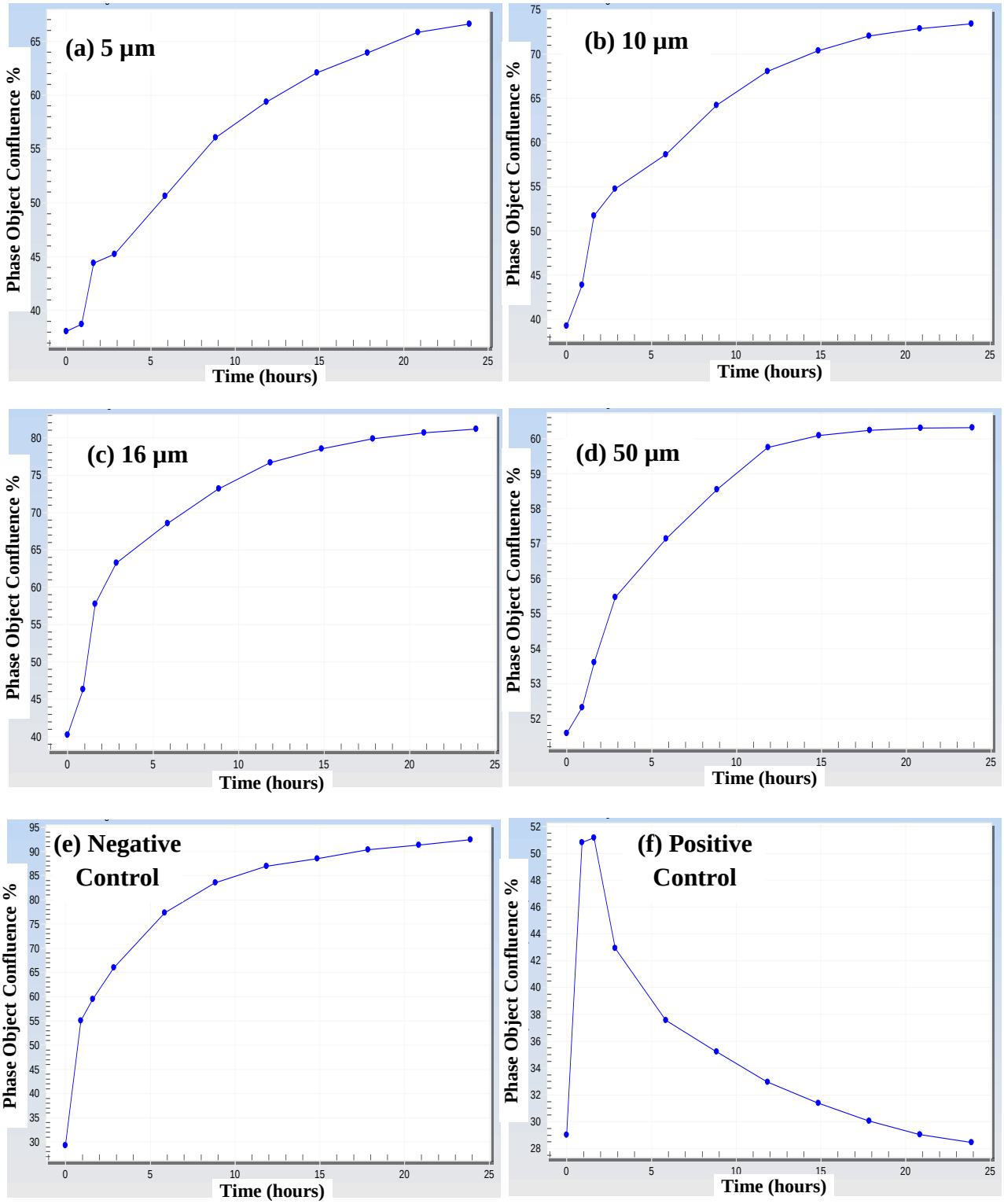

Figure 11: Growth of MC3T3 on CF-HIPed samples manufactured using a particle size of a) 5 µm, b) 10 µm, c) 16 µm , d) 50 µm and in presence of e) media (negative control) and f) hydrogen peroxide (positive control).

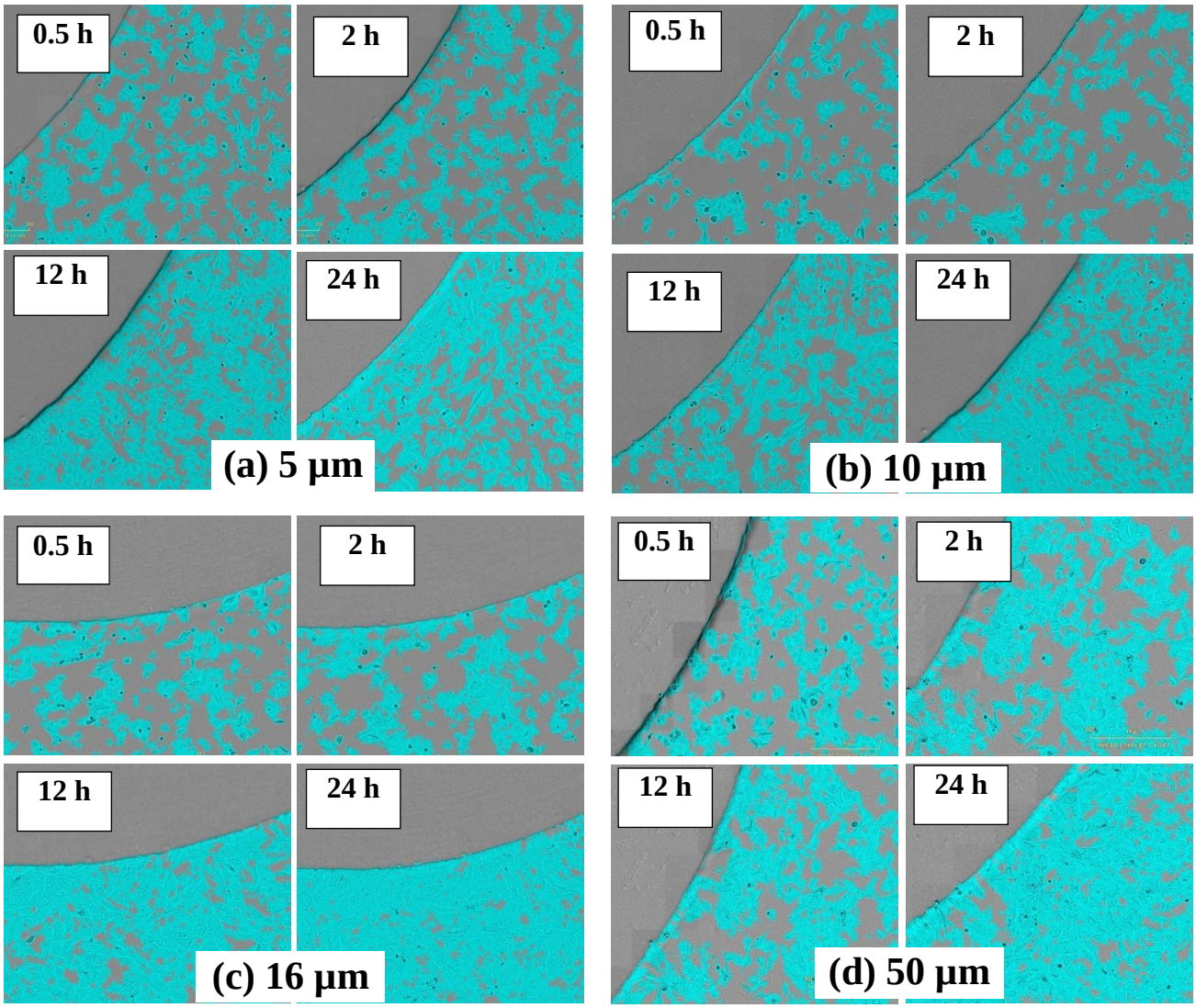

Figure 12: Images of MC3T3 growth at different time intervals on CF-HIPed samples manufactured using a particle size of a) 5 µm, b) 10 µm, c) 16 µm , d) 50 µm. Images are representative of 3 independent experiments.

5. Discussion

A cost effective CF-HIPing technology was successfully introduced to manufacture four different porous stainless steel 316L samples by using four different powder particle sizes. In all the prepared samples, CIPing and CF-HIPing process parameters (pressure, temperature, and hold time) were all kept constant. Therefore, the particle size was the only variable that affects the solid-state diffusion during CF-HIPing consolidation. This was supported by the microstructure and micro-CT imaging results as shown in Figure 4, Figure 5. In general, there was an increase in the porosity content, the pore size, and the interconnectivity between pores when the particle size increased. As shown in Figure 4, the porosity content of CF-HIPed samples prepared using particle size of 50 µm was the largest compared to the other three samples. Quantitative analysis of the porosity showed that the porosity content increased by 24% from 1.4% to 25.4% with the increase of the mean powder particle size from 5 µm to 50 µm. In addition, for all samples, the surface connected pores increased by increasing the particle size as shown in Figure 6.

It could be noted that the high porosity contents, the large pore size and the irregular pores, which were associated with the increase of the particle size, caused the deterioration in the mechanical properties of the samples. This is in agreement with the research by Kurgan [46] and Dewidar [47] who concluded a significant decrease in the mechanical properties of stainless steel 316L samples with the increase of porosity content. After analysing the mechanical properties, it can be noted that, samples prepared using powder particle size of 5 µm exhibits an increased Young's modulus (Figure 7 b), due the decreased porosity content. Young's modulus of 17–30 GPa, compressive strength of 107-190 MPa, and hardness of 25-28 HV can be achieved using implants prepared by particle of sizes between 32-50 µm (Figure 7). The Young's modulus and compressive strength values would be in a close range to that of human bone [48]. Furthermore, the high porosity content (17-25%) of the recommended implants would allow bone ingrowth, which could further stabilize the implants and would be favourable to avoid stress-shielding problems observed for solid bulk stainless steel implants [49], thus hence avoids implant loosening and promoting bone growth.

Generally, metallic biomaterials possess a wide range of mechanical properties such as fracture

toughness, ductility, high strength, formability and resistance to corrosion [50]. Nonetheless, metallic biomaterials devoid biological recognition on their surfaces, therefore, surface modification or surface coating are recommended to enhance biocompatibility. Besides, biomaterials of metallic origin can release toxic particles or ions leading to allergic and inflammatory reactions that cause loss of tissues. As discussed earlier, stainless steel has superior mechanical properties, nonetheless, it has lower resistance to corrosion compared to other implants; for instance titanium [51]. In addition, stainless steel content of nickel and high potential of allergic reactions makes it less biocompatible [52]. Around 80% or more of MC3T3 cells were healthy and viable for all CF-HIPed samples (Figure 12). CF-HIPed samples had a minimal toxic effect on the osteoblasts. These results are in agreement with the study conducted by Molders et al. [53], the study reported that some of the metal ions (Fe, Cr, Mo, Mn) released from the stainless steel can accumulate in the cells and disturb some cellular functions such as the bone morphogentic protein 2. Nonetheless, the study concluded that stainless steel samples used were biocompatible as it does not affect the growth of MC3T3-E1 cells as reflected by the Thiazolyl Blue assay (MTT assay).

The pore size range of the four scaffolds was comparable as demonstrated by the micro-CT imaging and cross-sectional SEM micrographs. Nonetheless, the percentage total porosities were significantly different. The live cell analysis showed that increasing the total percentage porosity was associated with increasing the proliferation of the osteoblasts. Samples prepared using 5 µm particles had the lowest total porosity of 1.4% and were associated with a slow growth rate. Increasing the percentage porosity to 11% and 12.9% respectively, was associated with increased proliferation of MC3T3 cells (Figure 12 b&c). The low porosity is believed to hinder the transport of nutrients and oxygen to the cells hence the lower proliferation in the 5 µm implants as suggested by Takahashi et al. [54].

On the other hand, high-density stainless steel could be achieved using particle size of 5 µm, which exhibited the best mechanical properties as compared to the other samples. The compressive strength of that samples was about 360 MPa which is similar to that of the bulk stainless steel 316L [44]. The presence of the surface porosity as shown in Figure 6a has one

additional benefit. If CF-HIPing route is to be used for dense structures, with only limited machining (in the order of <500 μm), will be required to remove the porous surface layer. Therefore, they are applicable in biomedical devices with less load-bearing capacity or other applications such as aerospace and automotive fields where high mechanical properties are favourable.

6. Conclusions

This study shows that the proposed CF-HIPing route was efficient to control the porosity of stainless steel parts and proved to be well-suited cost effective route for biomedical implants. It was found that CF-HIPed stainless steel samples of particle size between 5 and 50 μm had a porosity level varying from 1.4% to 25.4%, respectively. Variation of the porosity was found to have an impact on the mechanical and biological properties of the samples. In this respect, decreasing the powder particle size resulted in an improvement of the Young's modulus, compressive strength, and hardness of the CF-HIPed samples. By analysing the obtained properties and comparing them to human bone characteristics. It can be concluded that the proposed approach can be used to manufacture samples, which are appropriate for hard-tissue applications with Young's moduli between 17 and 30 GPa and high proliferation. The porosity fraction for those samples was 16 to 25.4% and the mechanical properties were 107 to 190 GPa for compressive strength, and from 25 to 28 HV for micro-hardness. An implant with such characteristics would be suitable for osseointegration. Thus, stress shielding can be prevented as the mechanical properties of the proposed materials are similar to that of human bone and the tissue growth could take place through the high level of interconnected pores, however, in vivo trials should be the next step. It is anticipated that the proposed approach could reduce the number of revision surgery. Finally, it is also worth to emphasise that although the aim of this work was mainly to develop porous structures, the results highlight the possibility of using the CF-HIPing approach to create highly dense structures, which can only be achieved using canisters with fine particle size. This limits the degree of surface connectivity, leaving behind a

porous surface region of ~100 μm, which can be later machined or electrochemically etched to generate a fully dense surface.

Conflicts of interest

In accordance with our policy on Conflicts of interest, the authors declares "There are no conflicts to declare".

References

1. *Global Health and Aging* N. I. o. Aging, World Health Organization, 2011.
2. O. Johnell and J. Kanis, *Osteoporosis International*, 2005, **16**, S3-S7.
3. T. P. van Staa, E. M. Dennison, H. G. M. Leufkens and C. Cooper, *Bone*, **29**, 517-522.
4. D. Tatkare, *World Medical Implants Market Opportunities and Forecasts*, Allied Market Research, Portland, United States, 2016.
5. J. Raphel, M. Holodniy, S. B. Goodman and S. C. Heilshorn, *Biomaterials*, 2016, **84**, 301-314.
6. S. Qian, Y. Qiao and X. Liu, *Journal of Materials Chemistry B*, 2014, **2**, 7475-7487.
7. L. Hao, L. Wei, L. Can, T. Jie, W. Hong, H. Bao, C. Hong, L. Hui-Jie, L. Zhong-Jun and S. Chun-Li, *Biofabrication*, 2016, **8**, 045012.
8. C. Alice, H. Aiza, J. C. David, D. B. Barbara and S. Zvi, *Biofabrication*, 2014, **6**, 045007.
9. H. Hassanin and K. Jiang, *Scripta Materialia*, 2013, **69**, 433-436.
10. J. Liu, Y. Yang, H. Hassanin, N. Jumbu, S. Deng, Q. Zuo and K. Jiang, *ACS Applied Materials & Interfaces*, 2016, **8**, 2607-2616.
11. S. C. Cox, P. Jamshidi, N. M. Eisenstein, M. A. Webber, H. Hassanin, M. M. Attallah, D. E. T. Shepherd, O. Addison and L. M. Grover, *Materials Science and Engineering: C*, 2016, **64**, 407-415.
12. J. Čapek, M. Machová, M. Fousová, J. Kubásek, D. Vojtěch, J. Fojt, E. Jablonská, J. Lipov and T. Ruml, *Materials Science and Engineering: C*, 2016, **69**, 631-639.
13. R. Fujisawa, M. Sakaihara, Y. Kurata and Y. Watanabe, *Corrosion Engineering, Science and Technology*, 2005, **40**, 244-248.
14. R. Wauthle, S. M. Ahmadi, S. Amin Yavari, M. Mulier, A. A. Zadpoor, H. Weinans, J. Van Humbeeck, J.-P. Kruth and J. Schrooten, *Materials Science and Engineering: C*, 2015, **54**, 94-100.
15. V. I. Kalita, D. I. Komlev, V. S. Komlev and A. A. Radyuk, *Materials Science and Engineering: C*, 2016, **60**, 255-259.
16. N. Taniguchi, S. Fujibayashi, M. Takemoto, K. Sasaki, B. Otsuki, T. Nakamura, T. Matsushita, T. Kokubo and S. Matsuda, *Materials Science and Engineering: C*, 2016, **59**, 690-701.
17. D. Hara, Y. Nakashima, T. Sato, M. Hirata, M. Kanazawa, Y. Kohno, K. Yoshimoto, Y. Yoshihara, A. Nakamura, Y. Nakao and Y. Iwamoto, *Materials Science and Engineering: C*, 2016, **59**, 1047-1052.
18. F. E. Wiria, J. Y. M. Shyan, P. N. Lim, F. G. C. Wen, J. F. Yeo and T. Cao, *Materials & Design*, 2010, **31, Supplement 1**, S101-S105.
19. I. R. Rustamov, V. A. Dyatlov, T. A. Grebeneva, A. V. Dyatlov, V. V. Zaitsev and V. I. Maleev, *Journal of Materials Chemistry B*, 2014, **2**, 4310-4317.
20. Y.-T. Liu, K.-C. Kung, C.-Y. Yang, T.-M. Lee and T.-S. Lui, *Journal of Materials Chemistry B*, 2014, **2**, 7927-7935.
21. T. Sonoda, K. Katou and T. Asahina, *Journal*, 2008, **591-593**, 277-281.
22. I. A. J. van Hengel, M. Riool, L. E. Fratila-Apachitei, J. Witte-Bouma, E. Farrell, A. A. Zadpoor, S. A. J. Zaat and I. Apachitei, *Biomaterials*, 2017, **140**, 1-15.
23. A. Fathy, A. Ahmed and H. Morgan, 2008.
24. L. P. Lefebvre, M. Gauthier and M. Patry, 2005.
25. J. Banhart, *Progress in Materials Science*, 2001, **46**, 559-632.
26. F. Dehghani and N. Annabi, *Current Opinion in Biotechnology*, 2011, **22**, 661-666.

27. V. Karageorgiou and D. Kaplan, *Biomaterials*, 2005, **26**, 5474-5491.
28. N. d. F. Daudt, M. Bram, A. P. C. Barbosa, A. M. Laptev and C. Alves Jr, *Journal of Materials Processing Technology*, 2017, **239**, 202-209.
29. C. Qiu, S. Yue, N. J. Adkins, M. Ward, H. Hassanin, P. D. Lee, P. J. Withers and M. M. Attallah, *Materials Science and Engineering: A*, 2015, **628**, 188-197.
30. K.-F. Lin, S. He, Y. Song, C.-M. Wang, Y. Gao, J.-Q. Li, P. Tang, Z. Wang, L. Bi and G.-X. Pei, *ACS Applied Materials & Interfaces*, 2016, **8**, 6905-6916.
31. M. K. Thompson, G. Moroni, T. Vaneker, G. Fadel, R. I. Campbell, I. Gibson, A. Bernard, J. Schulz, P. Graf, B. Ahuja and F. Martina, *CIRP Annals - Manufacturing Technology*, 2016, **65**, 737-760.
32. K. Essa, R. Khan, H. Hassanin, M. M. Attallah and R. Reed, *The International Journal of Advanced Manufacturing Technology*, 2016, **83**, 1835-1845.
33. C. Qiu, N. J. E. Adkins, H. Hassanin, M. M. Attallah and K. Essa, *Materials & Design*, 2015, **87**, 845-853.
34. W. Kim, J. E. Flinn and J. G. Byrne, *Acta Metallurgica et Materialia*, 1993, **41**, 49-57.
35. M. H. Bocanegra-Bernal, *Journal of Materials Science*, 2004, **39**, 6399-6420.
36. A. Abdelhafeez and K. Essa, *Procedia CIRP*, 2016, **55**, 188-193.
37. C. Qiu, N. Adkins, H. Hassanin, M. Attallah and K. Essa, *Materials & Design*, 2015.
38. J. Haan, M. Asseln, M. Zivcec, J. Eschweiler, R. Radermacher and C. Broeckmann, *Powder Metallurgy*, 2015, **58**, 161-165.
39. H. Wie, H. Herø and T. Solheim, *International Journal of Oral and Maxillofacial Implants*, 1998, **13**, 837-844.
40. H. Herø, H. Wie, R. B. Jørgensen and I. E. Ruyter, *Journal of Biomedical Materials Research*, 1994, **28**, 343-348.
41. I. Toshihiko, H. Shinya, S. Hideshi, S. Hodaka, Y. Yasutomo and Y. Masao, *Dental Materials Journal*, 2013, **32**, 274-280.
42. .
43. J. Breme, E. Eisenbarth and V. Biehl, in *Titanium and Titanium Alloys*, Wiley-VCH Verlag GmbH & Co. KGaA, 2005, DOI: 10.1002/3527602119.ch16, pp. 423-451.
44. A. ZoMMaterials, Stainless Steel - Grade 316 (UNS S31600), https://www.azom.com/properties.aspx?ArticleID=863, (accessed 05/11, 2017).
45. G. Repetto, A. del Peso and J. L. Zurita, *Nat. Protocols*, 2008, **3**, 1125-1131.
46. N. Kurgan, *Materials & Design*, 2014, **55**, 235-241.
47. M. Dewidar, *International Journal of Mechanical and Mechanics Engineering*, 2012, **12**, 10-24.
48. S. Bender, V. Chalivendra, N. Rahbar and S. El Wakil, *International Journal of Engineering Science*, 2012, **53**, 67-73.
49. B. Gervais, A. Vadean, M. Raison and M. Brochu, *Case Studies in Engineering Failure Analysis*, 2016, **5-6**, 30-38.
50. A. Nouri, P. D. Hodgson and C. e. Wen, in *Biomimetics Learning from Nature*, ed. A. Mukherjee, InTech, Rijeka, 2010, DOI: 10.5772/8787, p. Ch. 21.
51. I. Gotman, *Journal of Endourology*, 1997, **11**, 383-389.
52. J. A. Disegi and L. Eschbach, *Injury*, 2000, **31**, D2-D6.
53. M. Mölders, A. Fischer and M. Wiemann, *Materialwissenschaft und Werkstofftechnik*, 2002, **33**, 775-778.
54. Y. Takahashi and Y. Tabata, *Journal of Biomaterials Science, Polymer Edition*, 2004, **15**, 41-57.